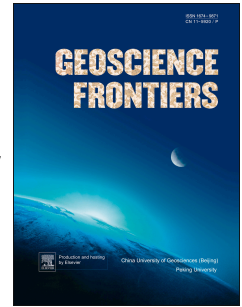


# Accepted Manuscript

Reintegrating nanogranitoid inclusion composition to reconstruct the prograde history of melt-depleted rocks

Omar Bartoli



PII: S1674-9871(18)30048-3

DOI: [10.1016/j.gsf.2018.02.002](https://doi.org/10.1016/j.gsf.2018.02.002)

Reference: GSF 673

To appear in: *Geoscience Frontiers*

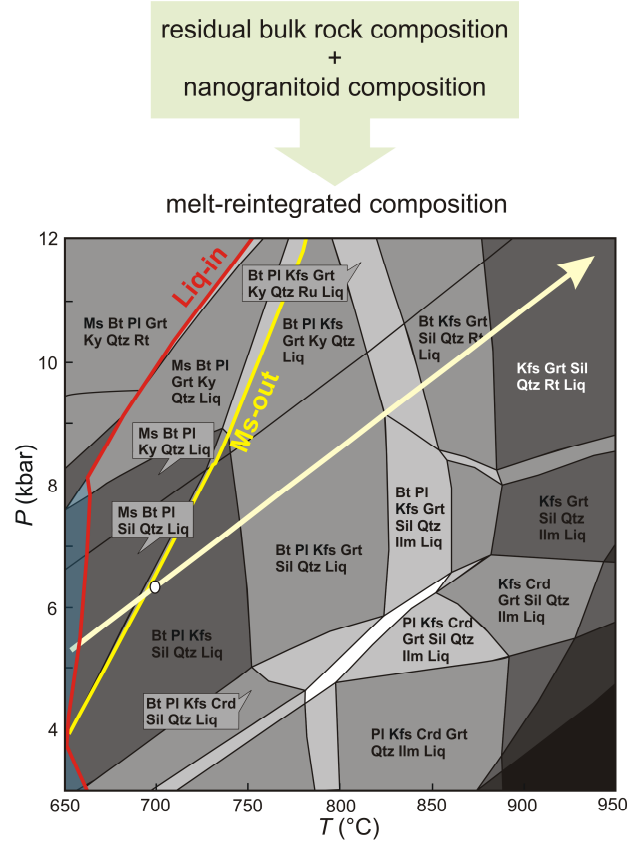
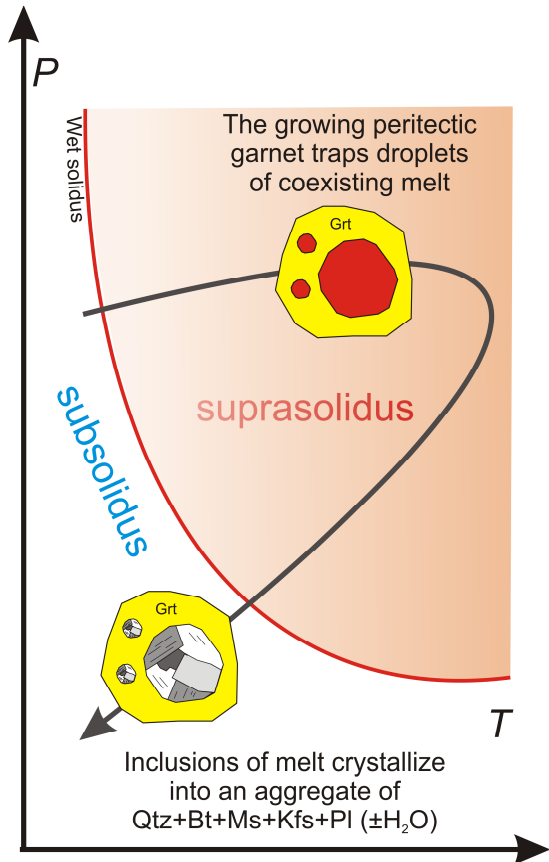
Received Date: 27 September 2017

Revised Date: 18 January 2018

Accepted Date: 7 February 2018

Please cite this article as: Bartoli, O., Reintegrating nanogranitoid inclusion composition to reconstruct the prograde history of melt-depleted rocks, *Geoscience Frontiers* (2018), doi: 10.1016/j.gsf.2018.02.002.

This is a PDF file of an unedited manuscript that has been accepted for publication. As a service to our customers we are providing this early version of the manuscript. The manuscript will undergo copyediting, typesetting, and review of the resulting proof before it is published in its final form. Please note that during the production process errors may be discovered which could affect the content, and all legal disclaimers that apply to the journal pertain.



ACCEPTED

## Reintegrating nanogranitoid inclusion composition to reconstruct the prograde history of melt-depleted rocks

**Omar Bartoli\***

*Department of Geosciences, University of Padova, Italy*

*\*Corresponding author. E-mail: omar.bartoli@unipd.it; omar.bartoli@libero.it*

### Abstract

A recent fascinating development in the study of high-grade metamorphic basements is represented by the finding of tiny inclusions of crystallized melt (nanogranitoid inclusions) hosted in peritectic phases of migmatites and granulites. These inclusions have the potential to provide the primary composition of crustal melts at the source. A novel use of the recently-published nanogranitoid compositional database is presented here. Using granulites from the world-renowned Ivrea Zone (NW Italy) on which the original melt-reintegration approach has been previously applied, it is shown that reintegrating melt inclusion compositions from the published database into residual rock compositions can be a further useful method to reconstruct a plausible prograde history of melt-depleted rocks. This reconstruction is fundamental to investigate the tectonothermal history of geological terranes.

**Keywords:** nanogranitoids, melt-reintegration, granulite, high-temperature metamorphism

## 1 **1. Introduction**

2 The deep continental crust has been ubiquitously affected by partial melting from  
3 Archean to present day in different geodynamic settings (Nehring et al., 2009; Sawyer  
4 et al., 2011). Loss of melt is a notoriously widespread process in crustal partially-  
5 melted rocks (Powell, 1983; White and Powell, 2002; Brown, 2007; Korhonen et al.,  
6 2010; Yakymchuk and Brown, 2014) and melt migration to upper crustal levels results  
7 in the formation of anatectic granites, leading to the geochemical differentiation of the  
8 Earth's crust (Brown and Rushmer, 2006). It follows that the study of melt-depleted  
9 rocks from the deep crust (residual migmatites and granulites) is key to understanding  
10 and characterizing the main processes that have promoted the chemical evolution of  
11 our planet (e.g. White and Powell, 2002; Guenrina and Sawyer, 2003; Morfin et al.,  
12 2013; Korhonen et al., 2015; Weinberg and Hasalová, 2015).

13 In the framework of natural crustal melts, a recent important advance is the  
14 finding of small crystallized melt inclusions (nanogranitoids) hosted in peritectic  
15 phases of migmatites and granulites (Fig. 1; Cesare et al., 2009, 2015; Ferrero et al.,  
16 2012; Bartoli et al., 2013a). When microstructurally, experimentally and  
17 microchemically investigated following precise procedures and protocols (Bartoli et  
18 al., 2013b; Cesare et al., 2015), these small data repositories can provide the primary  
19 composition of crustal melts at the source (Acosta-Vigil et al., 2010; Bartoli et al.,  
20 2014, 2016a; Ferrero et al., 2016a). The study and characterization of nanogranitoids  
21 have allowed significant advances in our understanding of crustal anatexis, such as a  
22 better comprehension of the melting mechanisms up to extreme UHP-UHT conditions  
23 (Acosta-Vigil et al., 2010, 2016; Bartoli et al., 2014, 2016a; Cesare et al., 2015;  
24 Ferrero et al., 2015, 2016a; Stepanov et al., 2016; Deng et al., 2017).

25 A geochemical database based on more than 600 nanogranitoid compositions

26 has been recently constructed: it comprises melt inclusions formed at conditions  
27 varying from 670 to 950 °C and 4 to 27 kbar, and found in metapelitic,metapsammitic  
28 and metagranitoid migmatites, and granulites (Cesare et al., 2015; Bartoli et al.,  
29 2016a). This dataset has been successfully used to track the processes involved in the  
30 chemical evolution of felsic magmas (e.g., fractional crystallization, cumulus  
31 phenomena, entrainment of peritectic phases, restiteunmixing; see Bartoli et al.,  
32 2016b). Experimental and modeling studies often refer to nanogranitoid compositions  
33 to complement and/or validate their inferences/results (e.g., Gao et al., 2016; Garcia-  
34 Arias and Stevens, 2017). Notably, Stepanov and Hermann (2013) used melt inclusion  
35 compositions from anatectic rocks to discuss an important and actively debated  
36 geochemical issue in the geological community such as the “missing Nb paradox”.

37 In this contribution an additional and novel use of the nanogranitoid  
38 compositional database is presented. Using granulites from the world-renowned Ivrea  
39 Zone (NW Italy) as an example, it is shown that reintegrating melt inclusion  
40 compositions from the published database into residual rock compositions can be  
41 considered a further useful method to reconstruct a plausible prograde history (melting  
42 conditions and reactions, and melt productivity) of melt-depleted rocks by means of  
43 phase equilibria modeling.

44 Bartoli (2017) has recently reviewed the different melt-reintegration  
45 approaches proposed in the literature. Whereas that manuscript provides a description  
46 and a comparative study of different procedures, in this contribution the utility of the  
47 published nanogranitoiddatabaseis illustrated in the framework of phase equilibria  
48 modeling of residual (melt-depleted) rocks.

49 Rocks from the Ivrea Zone have been chosen for three main reasons: (i) they  
50 represent a well-known and -studied anatecticterrane from amphibolite- to granulite-

51 facies conditions (Schmid and Wood, 1976; Zingg, 1980; Bea and Montero, 1999;  
52 Redler et al., 2012, 2013; Ewing et al., 2015); (ii) here, the melt-reintegration approach  
53 originally proposed by White et al. (2004) has been previously applied (Redler et al.,  
54 2013) and, therefore, a comparison between the two different methods can be done;  
55 and (iii) the precise protolith composition of these rocks is well-known allowing one to  
56 validate/invalidate the obtained results (Bartoli, 2017).

57

## 58 **2. Geological setting**

59 The Ivrea Zone (southern Alps of northwest Italy) is considered to represent a  
60 complete Permian mid to lower crustal section (Schmid, 1993; Barboza and Bergantz,  
61 2000). It comprises two main units: the Kinzigite Formation and the Mafic Complex  
62 (Quick et al., 2003). The Kinzigite Formation consists of a sequence of amphibolite to  
63 granulite facies rocks. The latter are associated with widespread anatexis, producing  
64 highly residual rocks (Schnetger, 1994; Redler et al., 2012, 2013). Metapelites are  
65 volumetrically dominant and are interlayered with metabasic rocks and minor  
66 calcsilicate rocks and marbles (Schmid, 1993; Redler et al., 2012; Kunz et al., 2014).  
67 Regional amphibolite to granulite facies metamorphism has been dated at c. 316Ma (U  
68 –Pb ages of zircon; Ewing et al., 2013). The reader may refer to Redler et al. (2012,  
69 2013) and Kunz et al. (2014) for a detailed petrographic description of rocks across the  
70 entire Kinzigite Formation.

71 The sample selected for this study comes from the Val Strona di Omegna which  
72 represents a section through amphibolite to granulite facies rocks (Fig. S1). Redler et al.  
73 (2012) modeled the stability fields for the inferred peak phase assemblages in different  
74 samples across the Val Strona di Omegna. These authors demonstrated that the sample  
75 set defines a continuous increase in pressure and temperature. The

76 obtained metamorphic gradient extends from conditions of 3.5–6.5 kbar at ~650 °C to  
77 10–12 kbar at > 900°C (Redler et al., 2012). Similar peak temperatures (900–930 °C)  
78 for the highest-grade rocks were obtained by zirconium-in-rutile thermometry (Ewing  
79 et al., 2013).

80

### 81 **3. Phase equilibria modeling**

82 Phase equilibria modeling represents a key methodology to study the tectonothermal  
83 history of geological terranes (White et al., 2007, 2017; Palin et al., 2016a, b). A  
84 widespread method to reconstruct the prograde history of melt-depleted rocks by  
85 means of phase equilibria modeling consists of (i) the addition of a certain amount of  
86 melt, whose composition is calculated at a given pressure and temperature, into the  
87 residual composition and (ii) performing phase equilibria modeling of the new model  
88 composition (White et al., 2004). Bartoli (2017) demonstrated that highly residual  
89 ( $\text{SiO}_2 < 55$  wt.%) compositions may affect somehow the feasibility of the melt-  
90 reintegration approach. Indeed, for these bulk rock compositions, the reintegration of a  
91 certain amount of melt up to the appearance of a  $\text{H}_2\text{O}$ -saturated solidus at the pressure  
92 of interest (i.e., the appearance of wet solidus has been generally used to determine the  
93 amount of melt to add back) does not guarantee the restoration of a reliable protolith  
94 composition, and the subsequent phase equilibria modeling of this model protolith may  
95 provide significant underestimations of melt productivity.

96 To avoid this drawback, the residual granulite IZ070 characterized by ~59 wt.%  
97 of  $\text{SiO}_2$  was selected for this study from the bulk rock compositions previously  
98 modeled by Redler et al. (2013). Because these authors applied the original melt-  
99 reintegration method, it is possible to compare the results obtained by the two different  
100 melt-reintegration procedures. Granulite IZ070 was collected in the highest-grade zone

101 of Val Strona di Omegna (Fig. S1). The peak mineral assemblage is composed of  
102 quartz, K-feldspar, garnet, sillimanite, ilmenite and rutile, and it is predicted to be  
103 stable at  $>850$  °C, 8–12 kbar (Redler et al., 2012, 2013).

104 Phase diagrams have been constructed using the Perple\_X software (Connolly,  
105 2009) with the thermodynamic database of Holland and Powell (1998, as revised in  
106 2003). The chemical system  $\text{Na}_2\text{O}-\text{CaO}-\text{K}_2\text{O}-\text{FeO}-\text{MgO}-\text{Al}_2\text{O}_3-\text{SiO}_2-\text{H}_2\text{O}-\text{TiO}_2$   
107 (NCKFMASHT) was selected. Ferric iron was ignored because its abundance in melt  
108 inclusions was not determined. Manganese was excluded because it has little effect on  
109 garnet-bearing equilibria at high-grade conditions (Redler et al., 2013). The solution  
110 model used are: melt from White et al. (2007), garnet from Holland and Powell (1998),  
111 biotite from Tajčmanová et al. (2009), white mica from Coggon and Holland (2002),  
112 plagioclase from Newton et al. (1980) and K-feldspar from Thompson and Hovis  
113 (1979). An ideal model was used for cordierite and ilmenite.

114 The first  $P-T$  pseudosection was calculated using the estimated residual bulk  
115 composition (Fig. 2a). Therefore, this diagram is only valid for assessing the peak and  
116 post-peak history (White et al., 2004). The peak conditions ( $>900$  °C, 10–12 kbar)  
117 inferred by Redler et al. (2012) correspond to a quadrivariant field in the high- $T$  part of  
118 the diagram containing the phase assemblage Kfs–Grt–Sil–Qtz–Rt–Liq (Fig. 2a), in  
119 agreement with the petrography observation of sample IZ070. The absence of  
120 ilmenite is likely due to the chosen  $\text{Fe}^{3+}$ -free chemical system (Dumond et al., 2015).  
121 Considering the proposed  $P-T$  evolution, the solidus is encountered at  $\sim 850$  °C and  $\sim 9$   
122 kbar.

123 The main stages of melt production in Ivrea Zone granulites are expected to  
124 occur at  $\sim 650-700$  °C via muscovite breakdown and from  $\sim 750$  to  $\sim 850$  °C via biotite  
125 breakdown (Redler et al., 2013). In applying melt-reintegration methodology some



126 approximations, such as the number of melt-reintegration steps and the amount of melt  
127 to be added back at each step, are needed because it is impossible to retrieve the real  
128 melt loss history of crustal rocks. In the case of Ivrea Zone rocks, three melt-  
129 reintegration steps (Fig. 2b–d) were performed along a schematic  $P$ – $T$  path where an  
130 amount of melt, sufficient to promote melt drainage and loss, is expected to have been  
131 produced on the basis of field and petrographic observations, and phase equilibria  
132 constraints (Fig. 10 in Redler et al., 2013) –i.e., at  $\sim 700$  °C and  $\sim 6$  kbar where  
133 muscovite is likely to have been totally consumed in these rocks (i.e., at the likely  
134 maximum temperature at which muscovite-melting derived melts have been produced),  
135 and at 800 °C (during biotite dehydration melting) and at 850 °C,  $\sim 8$ – $10$  kbar (i.e.,  
136 close to the Bt-out reaction). Melt inclusion compositions appropriate for these  
137 conditions were selected from the geochemical database published in Cesare et al.  
138 (2015) and Bartoli et al. (2016a). The  $P$ – $T$  conditions of melt inclusion formation were  
139 determined by different methods (i.e., remelting experiments, phase equilibria  
140 modeling, classic thermobarometry, trace element thermometry) or by a combination  
141 of them (Cesare et al., 2015 and references therein). Because the composition of the  
142 source rock may exert a control on the composition of anatectic melts, nanogranitoids  
143 found in metapelitic rocks were selected for this study (Fig. S2).

144 The bulk compositions used to calculate pseudosections as well as the  
145 compositions of reintegrated melts and their inferred  $P$ – $T$  conditions of formation are  
146 reported in Table 1. Melt inclusions formed at higher temperature generally show  
147 higher FeO, CaO and K<sub>2</sub>O contents and lower H<sub>2</sub>O amounts (Table 1).

148 At each melt-reintegration step, a certain amount of melt was added back until  
149 melt persisted to conditions appropriate for the next reintegration. For example, 27  
150 wt.% melt formed at  $\sim 850$  °C was added back to the residuum composition until

151 solidus appeared at  $\sim 800$  °C and  $\sim 8$  kbar (Fig.2b). Then, 20 wt.% melt was  
152 reintegrated at 800 °C (Fig. 1c). In agreement with the melt-reintegration modeling  
153 performed by Redler et al. (2013) and the assumed  $P$ - $T$  path, an amount of melt  
154 sufficient to produce a  $H_2O$ -saturated solidus at  $T < 700$  °C and at  $P \sim 7$  kbar was added  
155 back during the last melt-reintegration step at 700 °C (Fig.2d). Once melt-reintegration  
156 procedure has been completed, the most evident changes in the phase diagram  
157 topology are (i) the shift of the solidus to lower temperatures, (ii) the  $H_2O$ -saturated  
158 character of solidus curve at  $P < 8$  kbar, and (iii) the appearance of muscovite-bearing  
159 subsolidus and suprasolidus assemblages (Fig. 2).

160 The final model protolith composition (IZ070c) overlaps the composition of  
161 amphibolite-facies rocks which are considered to reflect the composition of the  
162 protoliths of granulite-facies rocks (Fig. 3). Therefore, the approach proposed in this  
163 study ensures the restoration of a reliable protolith composition.

164

## 165 **4. Discussion**

### 166 *4.1. Comparison with the original melt-reintegration approach*

167 In the original melt-reintegration method proposed by White et al. (2004), melt was  
168 added back at conditions of the original solidus calculated with the observed bulk  
169 composition until melt persisted to lower temperatures. The procedure was repeated so  
170 that the lower temperature boundary of each phase assemblage field involves the  
171 appearance of melt, until a free fluid was present beyond the solidus (Bartoli, 2017).  
172 Redler et al. (2013) applied this method to the melt-depleted rocks IZ070 and IZ020  
173 from the granulite-facies and transition zones, respectively. Their model protolith  
174 composition for the highest grade rock (IZ070Re) plots inside the compositional field  
175 of amphibolite-facies rocks (Fig. 3) and displays some compositional similarities with

176 respect to the protolith composition IZ070c reconstructed in this study (Fig. 3). For  
177 instance,  $\text{Al}_2\text{O}_3$ ,  $\text{CaO}$ ,  $\text{K}_2\text{O}$  and  $\text{H}_2\text{O}$  are < 10 wt.% relative higher in IZ070Re sample,  
178 whereas  $\text{SiO}_2$  is 6 wt.% relative lower. As a consequence, the topology of  $P$ - $T$   
179 pseudosection constructed using the protolith composition IZ070Re is very similar to  
180 that obtained in this study for the bulk composition IZ070c (Fig. S3). Also, a number  
181 of similarities in the first-order topology can be seen in Fig. 2d and the original  $P$ - $T$   
182 pseudo section calculated by Redler et al. (2013) using THERMOCALC. In the latter  
183 case, ilmenite is predicted to be stable at peak conditions owing to the involvement of  
184  $\text{Fe}^{3+}$  as chemical component (Fig. 9b in Redler et al., 2013).

185 Fig. 4 shows the calculated phase amounts for the model protolith compositions  
186 IZ070c and IZ070Re. Considering the uncertainties associated with phase equilibria  
187 modeling and the assumptions made to apply melt-reintegration approaches (Palin et  
188 al., 2016a; Bartoli, 2017; Koblinger and Pattison, 2017), it is clear that the phase  
189 amounts predicted along the prograde  $P$ - $T$  path considerably match each other (Fig. 4).  
190 On the other hand, some discrepancies seem to exist when compositional isopleths are  
191 compared, in particular for  $X_{\text{An}}[\text{Ca}/(\text{Ca}+\text{Na})]$  of plagioclase (Fig. 5). This makes sense,  
192 because the composition of feldspars is particularly sensitive to the melt  
193 composition. Despite these discrepancies overlap with the intrinsic uncertainties related  
194 to phase equilibria calculations (Powell and Holland, 2008; Angiboust et al., 2012;  
195 Palin et al., 2012; Koblinger and Pattison, 2017), the above results suggest that the  
196 feldspar compositional isopleths should not be considered to derive the  $P$ - $T$  constraints  
197 once the melt-reintegration approach is applied.

198

199

200 4.2. Reintegrating composition of natural melts

201 Melt-reintegration approach has been routinely applied on a variety of melt-depleted  
202 rocks. In the majority of previous studies, the composition of melt to be reintegrated  
203 has been calculated by phase equilibria modeling, even though different ways of  
204 reintegrating calculated melt compositions have been proposed in the literature  
205 (reviewed by Bartoli, 2017). Recently, some authors have proposed to reintegrate  
206 natural melt compositions, rather than melt compositions calculated by thermodynamic  
207 modeling. For example, Anderson et al. (2013) investigated the high-grade  
208 metamorphism in the Anmatjira Range (Arunta region, central Australia). These  
209 authors calculated an average crustal melt composition using published S-type granite  
210 compositions derived from melting of aluminous rocks. This average leucogranite  
211 composition was then used to construct a  $T$ - $M_{\text{melt}}$  section which was successfully  
212 applied to reconstruct the pre-melt loss bulk composition of the investigate rock (cf.  
213 Fig. 7 in Anderson et al., 2013). On the other hand, Wang and Guo (2017) reintegrated  
214 the average bulk composition of six leucosomes enclosed in residual HP granulites  
215 from the Yinshan Block (North China Craton).

216 Despite the composition of leucogranites and leucosomes has provided  
217 fundamental clues on the crustal melting mechanisms and geochemical differentiation  
218 of Earth's crust (e.g., Deniel et al., 1987; Stevens et al., 2007; Villaros et al., 2009;  
219 Zeng et al., 2005), they rarely reflect primary (i.e. unmodified) crustal melts. Rather  
220 the composition of these rocks may be variably affected by fractional crystallization  
221 process, accumulation of early-crystallized minerals, selective entrainment of residual  
222 and/or peritectic phases and wholesale entrainment of non-protolithologies  
223 (Chappell et al., 1987; Milord et al., 2001; Stevens et al., 2007; Sawyer, 2008, 2014;  
224 Clemens and Stevens, 2012; Brown et al., 2016; Carvalho et al., 2016, 2017). For these  
225 reasons, the composition of experimental glasses has been commonly assumed as

226 representative of melt composition at the source and used for geochemical  
227 considerations on anatectic terranes(e.g., Milord et al., 2001; Guernina and Sawyer,  
228 2003; Carvalho et al., 2016). It is important to notice that the aforementioned studies  
229 adopted the same approach of this study (i.e., the used experimental melt compositions  
230 produced from starting material and at  $P$ - $T$  conditions closest to the investigated rock).

231 Recently, the appearance of the compositional database of nanogranitoid  
232 inclusions has provided an additional useful geochemical tool (Bartoli et al., 2016a).  
233 For example, both the compositions of melt inclusions and experimental glasses have  
234 been considered to track the processes that control the leucosome compositions in  
235 metasedimentary granulites from the Limpopo Belt, South Africa (Taylor et al., 2014).

236

## 237 **5. Future perspectives**

### 238 *5.1. Using the published compositional database*

239 This study demonstrates that reintegrating the composition of nanogranitoid inclusions  
240 from the published geochemical database into residual bulk rock compositions can be  
241 considered an additional useful method to reconstruct the prograde history of melt-  
242 depleted rocks by means of phase equilibria modeling. Adding back natural melt  
243 compositions may be a way to reduce the gap between natural systems and  
244 models which represents, instead, simplified proxies of natural occurrences. In Fig. 6,  
245 the reintegrated compositions of melt inclusions are compared with the melt  
246 compositions calculated from the thermodynamic modeling at the same conditions.  
247 Nanogranitoids generally show higher FeO, MgO and lower Al<sub>2</sub>O<sub>3</sub> and Na<sub>2</sub>O. CaO and  
248 K<sub>2</sub>O are variable. It could be argued that such differences are related to the use of  
249 nanogranitoid inclusions not coming from the investigated rock. However, a similar  
250 discrepancy—between calculated and measured melt compositions—has been already

251 reported in other anatectic terranes (Bartoli et al., 2013c, 2016b) and in experimental  
252 runs (Grant, 2009), and seems to be related to the current melt model which needs  
253 some improvements (see White et al., 2011). Notably, the extent of the compositional  
254 discrepancy found in this study recalls that previously observed between nanogranitoids  
255 and calculated melts coming from the same rock and formed at the same  $P$ - $T$   
256 conditions (Fig. 6).

257         Although the selected nanogranitoid compositions do not reflect the precise  
258 composition of melt produced in the investigated rock from Ivrea Zone, this study  
259 supports the inferences by Bartoli et al. (2016a) that using the melt inclusion  
260 compositions from the published data set for the conditions ( $P$ - $T$ -bulk rock  
261 composition) closest to the investigated rock is a valid assumption which provide  
262 reliable results. This outcome is very important because melt inclusions are not present  
263 in all anatectic terranes worldwide. Notably, the published nanogranitoid database  
264 (Cesare et al., 2015; Bartoli et al., 2016a) is continuously being updated. For instance,  
265 Ferrero et al. (2018) recently recovered the composition of nanogranitoid inclusions  
266 from ultramafic granulites.

267

## 268 *5.2. Some assumptions are unavoidably needed*

269         Ivrea Zone has been intensively investigated during the past four decades and  
270 the  $P$ - $T$  evolution of migmatites and granulites is pretty well constrained (see above).  
271 However, in other anatectic terranes the prograde  $P$ - $T$  path may be rather uncertain  
272 and, in turn, deciding the number of melt-reintegration steps and the  $P$ - $T$  conditions  
273 where melt should be added back can be not trivial. Some hints to recover the probable  
274  $P$ - $T$  evolution and, in turn, the possible melt-forming reactions may come from the  
275 tectonic model of the investigated areas and/or petrographic constraints. For example,

276 felsic granulites from the Athabasca Granulite Terrane (Canada) show textural  
277 evidence suggesting minimum peak conditions of >14 kbar and >925 °C (Dumond et  
278 al., 2015). In agreement with the geology of the area, Dumond et al. (2015) inferred a  
279  $P$ - $T$  path corresponding to the prograde burial of sediments to a depth in excess of 50  
280 km along which melt was reintegrated four times where the  $P$ - $T$  path crossed the 1  
281 mol.% melt isopleth.

282 On the other hand, Korhonen et al. (2013) constrained peak conditions for  
283 granulites from the Eastern Ghats Province (India) combining petrographic  
284 observations (i.e., identifying the peak phase assemblage) and phase equilibria  
285 calculations for the residual bulk rock composition. Then, these authors assumed a  
286 prograde  $P$ - $T$  path of 150 °C/kbar for the melt reintegration procedure (Korhonen et  
287 al., 2013). Such a  $P$ - $T$  evolution is considered typical of regions which experienced  
288 UHT conditions (Brown, 2006, 2007; Kelsey and Hand, 2014).

289 On the basis of the reached thermal peak (i.e., high or low suprasolidus  
290 temperatures), one can decide to perform one or more melt-reintegration steps,  
291 similarly to what done by Morrissey et al. (2016) to model multiple melt loss events  
292 (which consists in the inverse approach of melt-reintegration method). These authors  
293 assumed a  $P$ - $T$  path and modeled three melt loss events: on the wet solidus and on the  
294 muscovite- and biotite-out curves.

295

### 296 *5.3. Reconstruction of a plausible effective bulk composition*

297 Residual bulk rock compositions can be inadequate to model the entire  
298 prograde history not only for the previous extraction of some batches of melt resulting  
299 in a residual bulk rock composition, but also for the occurrence of large, chemically  
300 zoned porphyroblasts which can cause chemical fractionation during their growth,

301 changing the chemical composition of the reacting rock volume (Marmo et al., 2002;  
302 Evans, 2004). In such a case, different effective bulk compositions have to be  
303 considered to model different steps along the  $P$ - $T$  path, modifying the bulk rock  
304 composition according to the predicted element incorporation in the fractionated  
305 mineral (Gaidies et al., 2006; Konrad-Schmolke et al., 2008; Groppo et al., 2009;  
306 Iaccarino et al., 2017). Occasionally, nanogranitoid inclusions show a systematic  
307 distribution in annuli around a melt inclusion-free garnet core (Fig. 7a; Carosi et al.,  
308 2015; Cesare et al., 2015). When this occurrence is associated with low melting  
309 temperature ( $<750$  °C) or short duration of HT metamorphism preventing a complete  
310 chemical re-equilibration of garnet prophyro blasts (i.e., a complete diffusive resetting;  
311 Caddick et al., 2010), the reconstruction of a plausible effective bulk composition for  
312 the melting event can take advantage of both the reintegration of melt inclusion  
313 composition and the removal of elements fractionated in the subsolidus garnet core  
314 (Fig. 7a).

315

#### 316 *5.4. Modeling distinct anatexis events within a single rock*

317 High-grade metamorphic terranes often show a polymetamorphic history  
318 related to one or more orogenic cycles (Korhonen et al., 2010; Ewing et al., 2015;  
319 Yakymchuk et al., 2015). Sometimes it is possible to find evidence of two distinct  
320 anatexis events within a single garnet crystal. For example, garnet from granulitic  
321 migmatites of the sequence of Jubrique (Betic Cordillera, S Spain) contains granitic  
322 melt inclusions associated to kyanite and rutile in the core, whereas granodioritic to  
323 tonalitic melt inclusions are associated to sillimanite and ilmenite at the rim of the host  
324 crystal (Fig. 7b; Barich et al., 2014; Acosta-Vigil et al., 2016). Clearly, this  
325 nanogranitoid occurrence will allow one to pursue an unique approach: the



326 reintegration of the right melt composition for each anatectic event to be modeled.

327

## 328 **6. Concluding remarks**

329 Most granulitic terranes worldwide experienced loss of anatectic melt, resulting in  
330 residual bulk rock compositions. Although the investigated rock does not contain melt  
331 inclusions, reintegrating the composition of nanogranitoid inclusions from the  
332 published geochemical database, for the conditions (*P-T*-bulk rock composition)  
333 closest to the investigated rock, can be considered an additional useful method to  
334 reconstruct the prograde history of melt-depleted rocks by means of phase equilibria  
335 modeling.

336

## 337 **Acknowledgements**

338 This research was supported by the Italian Ministry of Education, University, Research  
339 (Grant SIR RBSI14Y7PF to O.B.). I am grateful to F. Korhonen, S. Iaccarino,  
340 A. Langone and an anonymous referee for providing insightful and constructive  
341 reviews. Associated Editor Dr. C. Spencer is thanked for his careful editorial handling.

342

343

## 344 **References**

- 345 Acosta-Vigil, A., Buick, I., Hermann, J., Cesare, B., Rubatto, D., London, D., Morgan  
346 VI, G.B., 2010. Mechanisms of crustal anatexis: a geochemical study of partially  
347 melted metapelitic enclaves and host dacite, SE Spain. *Journal of Petrology* 51, 785–  
348 821.
- 349 Acosta-Vigil, A., Barich, A., Bartoli, O., Garrido, C., Cesare, B., Remusat, L., Poli, S.,  
350 Raepsaet, C., 2016. The composition of nanogranitoids in migmatites overlying the  
351 Ronda peridotites (Betic Cordillera, S Spain): the anatectic history of a  
352 polymetamorphic basement. *Contributions to Mineralogy and Petrology* 171, 24.
- 353 Anderson, J. R., Kelsey, D. E., Hand, M., Collins, W. J., 2013. Conductively driven,  
354 high-thermal gradient metamorphism in the Anmatjira Range, Arunta region, central  
355 Australia. *Journal of Metamorphic Geology* 31, 1003–1026.
- 356 Angiboust, S., Langdon, R., Agard, P., Waters, D., Chopin, C., 2012. Eclogitization of  
357 the Monviso ophiolite (W. Alps) and implications on subduction dynamics. *Journal of*  
358 *Metamorphic Geology* 30, 37–61.
- 359 Barboza, S.A., Bergantz, G.W., 2000. Metamorphism and anatexis in the Mafic  
360 Complex contact aureole, Ivrea Zone, Northern Italy. *Journal of Petrology* 41, 1307–  
361 1327.
- 362 Barich, A., Acosta-Vigil A., Garrido, C.J., Cesare, B., Tajčmanová, L., Bartoli, O.

- 363 2014. Microstructures and petrology of melt inclusions in the anatectic sequence of  
364 Jubrique (Betic Cordillera, S Spain): implications for crustal anatexis. *Lithos* 206–  
365 207, 303–320.
- 366 Bartoli, O., 2017. Phase equilibriamodeling of residual migmatites and granulites: an  
367 evaluation of the melt-reintegration approach. *Journal of Metamorphic Geology* 35,  
368 919–942.
- 369 Bartoli, O., Cesare, B., Poli, S., Bodnar, R.J., Acosta-Vigil, A., Frezzotti, M.L., Meli,  
370 S., 2013a. Recovering the composition of melt and the fluid regime at the onset of  
371 crustal anatexis and S-type granite formation. *Geology* 41, 115–118.
- 372 Bartoli, O., Cesare, B., Poli, S., Acosta-Vigil, A., Esposito, R., Turina, A., Bodnar,  
373 R.J., Angel, R.J., Hunter, J., 2013b. Nanogranite inclusions in migmatitic garnet:  
374 behavior during piston cylinder re-melting experiments. *Geofluids* 13, 405–420.
- 375 Bartoli, O., Tajčmanová, L., Cesare, B., Acosta-Vigil, A., 2013c. Phase equilibria  
376 constraints on melting of stromatic migmatites from Ronda (S. Spain): Insights on the  
377 formation of peritectic garnet. *Journal of Metamorphic Geology* 31, 775–789.
- 378 Bartoli, O., Cesare, B., Remusat, L., Acosta-Vigil, A., Poli, S., 2014. The H<sub>2</sub>O content  
379 of granite embryos. *Earth and Planetary Science Letters* 395, 281–290.
- 380 Bartoli, O., Acosta-Vigil, A., Ferrero, S., Cesare, B., 2016a. Granitoid magmas  
381 preserved as melt inclusions in high-grade metamorphic rocks. *American*  
382 *Mineralogist* 101, 1543–1559.
- 383 Bartoli, O., Acosta-Vigil, A., Tajčmanová, L., Cesare, B., Bodnar, R. J., 2016b. Using  
384 nanogranitoids and phase equilibria modeling to unravel anatexis in the crustal  
385 footwall of the Ronda peridotites (Betic Cordillera, S Spain). *Lithos* 256–257, 282–  
386 299.
- 387 Brown, M., 2006. Duality of thermal regimes is the distinctive characteristic of plate  
388 tectonics since the Neoproterozoic. *Geology* 34/11, 961–964.
- 389 Brown, M., 2007. Crustal melting and melt extraction, ascent and emplacement in  
390 orogens: mechanisms and consequences. *Journal of Geological Society, London*, 164,  
391 709–730.
- 392 Brown, M., Rushmer, T., 2006. *Evolution and differentiation of the continental crust*.  
393 Cambridge University Press, pp. 296–331.
- 394 Brown, C.R., Yakymchuk, C., Brown, M., Fanning, C.M., Korhonen, F.J., Piccoli,  
395 P.M., Siddoway, C.S., 2016. From source to sink: petrogenesis of Cretaceous  
396 anatectic granites from the Fosdick migmatite-granite complex, West Antarctica.  
397 *Journal of Petrology* 57, 1241–1278.
- 398 Caddick, M.J., Konopásek, J., Thompson, A.B., 2010. Preservation of garnet growth  
399 zoning and the duration of prograde metamorphism. *Journal of Petrology* 51, 2327–  
400 2347.
- 401 Carosi, R., Montomoli, C., Langone, A., Turina, A., Cesare, B., Iaccarino, S., Fascioli,  
402 L., Visonà, D., Ronchi, A., Rai, S. M. 2015. Eocene partial melting recorded in  
403 peritectic garnets from kyanite-gneiss, Greater Himalayan Sequence, central Nepal.  
404 In: Mukherjee S, Carosi R, van der Beek PA, Mukherjee BK, Robinson DM (eds)  
405 *Tectonics of the Himalaya*. Geological Society, London, Special Publications 412,  
406 111–129
- 407 Carvalho, B.B., Sawyer, E.W., Janasi, V.A., 2016. Crustal reworking in a shear zone:  
408 transformation of metagranite to migmatite. *Journal of Metamorphic Geology* 34, 237–  
409 264.
- 410 Carvalho, B.B., Sawyer, E.W., Janasi, V.A., 2017. Enhancing maficity of granitic  
411 magma during anatexis: entrainment of infertile mafic lithologies. *Journal of Petrology*  
412 58, 1333–1362.

- 413 Cesare, B., Ferrero, S., Salvioli-Mariani, E., Pedron, D., Cavallo, A., 2009. Nanogranite  
 414 and glassy inclusions: the anatectic melt in migmatites and granulites. *Geology*  
 415 37, 627–630.
- 416 Cesare, B., Acosta-Vigil, A., Bartoli, O., Ferrero, S., 2015. What can we learn from  
 417 melt inclusions in migmatites and granulites? *Lithos* 239, 186–216.
- 418 Chappell, B.W., White, A.J.R., Wyborn, D., 1987. The importance of residual source  
 419 material (Restite) in granite petrogenesis. *Journal of Petrology*, 28, 1111–1138.
- 420 Clemens, J.D., Stevens, G., 2012. What controls chemical variation in granitic  
 421 magmas? *Lithos* 134-135, 317–329.
- 422 Coggon, R., Holland, T. J. B., 2002. Mixing properties of phengitic micas and revised  
 423 garnet–phengite thermobarometers. *Journal of Metamorphic Geology* 20, 683–696.
- 424 Connolly, J.A.D., 2009. The geodynamic equation of state: What and how.  
 425 *Geochemistry, Geophysics, Geosystems*, 10, Q10014.
- 426 Deniel, C., Vidal, P., Fernandez, A., LeFort, P., Pecaut, J.J., 1987. Isotopic study of the  
 427 Manaslu granite (Himalaya, Nepal): inferences of the age and source of Himalayan  
 428 leucogranites. *Contributions to Mineralogy and Petrology* 96, 78–92.
- 429 Deng, L-P., Liu, Y-C., Gu, X-F., Groppo, C., Rolfo, F., 2017. Partial melting of  
 430 ultrahigh-pressure metamorphic rocks: evidences, melt compositions and physical  
 431 effects. *Geoscience Frontiers*, doi: 10.1016/j.gsf.2017.08.002.
- 432 Dumond, G., Goncalves, P., Williams, M.L., Jercinovic, M.J., 2015. Monazite as a  
 433 monitor of melting, garnet growth and feldspar recrystallization in continental lower  
 434 crust. *Journal of Metamorphic Geology* 33, 735–762.
- 435 Evans, T. P., 2004. A method for calculating effective bulk composition modification  
 436 due to crystal fractionation in garnet-bearing schist: implication for  
 437 isopleth thermobarometry. *Journal of Metamorphic Geology* 22, 547–557.
- 438 Ewing, T.A., Hermann, J., Rubatto, D., 2013. The robustness of the Zr-in-rutile and Ti-  
 439 in-zircon thermometers during high-temperature metamorphism (Ivrea-Verbanzone,  
 440 northern Italy). *Contributions to Mineralogy and Petrology* 4, 757–779.
- 441 Ewing, T.A., Rubatto, D., Beltrando, M., Hermann, J., 2015. Constraints on the thermal  
 442 evolution of the Adriatic margin during Jurassic continental break-up: U–Pb dating of  
 443 rutile from the Ivrea–Verbanzone, Italy. *Contributions to Mineralogy and*  
 444 *Petrology* 169:44.
- 445 Ferrero, S., Bartoli, O., Cesare, B., Salvioli-Mariani, E., Acosta-Vigil, A., Cavallo, A.,  
 446 Groppo, C., Battiston, S., 2012. Microstructures of melt inclusions in anatectic  
 447 metasedimentary rocks. *Journal of Metamorphic Geology* 30, 303–322.
- 448 Ferrero, S., Wunder, B., Walczak, K., O'Brien, P.J., Ziemann, M.A., 2015. Preserved  
 449 near ultrahigh-pressure melt from continental crust subducted to mantle depths.  
 450 *Geology* 43, 447–450.
- 451 Ferrero, S., Wunder, B., Ziemann, M.A., Wälle, M., O'Brien, P.J., 2016.  
 452 Carbonatitic and granitic melts produced under conditions of primary immiscibility  
 453 during anatexis in the lower crust. *Earth and Planetary Science Letters* 454, 121–131.
- 454 Ferrero, S., Godard, G., Palmeri, R., Wunder, B., Cesare, B., 2018. Partial melting of  
 455 ultramafic granulites from Dronning Maud Land, Antarctica: constraints from melt  
 456 inclusions and thermodynamic modeling. *American Mineralogist*, submitted.
- 457 Gaidies, F., Abart, R., De Capitani, C., Schuster, R., Connolly, J.A.D., Reusser, 2006.  
 458 Characterization of polymetamorphism in the Austroalpine basement east of the  
 459 Tauern Window using garnet isopleth thermobarometry. *Journal of Metamorphic*  
 460 *Geology* 24, 451–475.
- 461 Gao P., Zheng, Y-F., Zhao Z-F., 2016. Experimental melts from crustal rocks: A  
 462 lithochemical constraint on granite petrogenesis. *Lithos* 266–267, 133–157.

- 463 Garcia-Arias, M., Stevens, G., 2017. Phase equilibrium modelling of granite magma  
464 petrogenesis: A. An evaluation of the magma compositions produced by crystal  
465 entrainment in the source. *Lithos*, 277, 131–153.
- 466 Grant, J.A., 2009. THERMOCALC and experimental modelling of pelite, Morton  
467 Pass, Wyoming. *Journal of Metamorphic Geology* 27, 571–578.
- 468 Groppo, C., Rolfo, F., Lombardo, B., 2009. P-T evolution across the Main Central  
469 Thrust Zone (Eastern Nepal): hidden discontinuities revealed by petrology. *Journal of*  
470 *Petrology*, 50, 1149–1180.
- 471 Guernina, S., Sawyer, E.W., 2003. Large-scale melt-depletion in granulite terranes: an  
472 example from the Archean Ashuanipisubprovince of Quebec. *Journal of Metamorphic*  
473 *Geology* 21, 181–201.
- 474 Holland, T.J.B., Powell, R., 1998. An internally consistent thermodynamic data set for  
475 phases of petrological interest. *Journal of Metamorphic Geology* 16, 309–343.
- 476 Holland, T.J.B., Powell, R., 2003. Activity-composition relations for phases in  
477 petrological calculations: An asymmetric multicomponent formulation. *Contributions*  
478 *to Mineralogy and Petrology*, 145, 492–501.
- 479 Kelsey, D. E., and Hand, M., 2014. On ultrahigh temperature crustal metamorphism:  
480 Phase equilibria, trace element thermometry, bulk composition, heat sources,  
481 timescales and tectonic settings. *Geoscience Frontiers* 6, 311–356.
- 482 Koblinger, B.M., Pattison, D.R.M., 2017. Crystallization of heterogeneous  
483 pelitic migmatites: insights from thermodynamic modeling. *Journal of Petrology* 58–  
484 2, 297–326
- 485 Konrad-Schmolke, M., O'Brien, P.J., de Capitani, C., Carswell, D.A., 2008. Garnet  
486 growth at high- and ultra-high pressure conditions and the effect of element  
487 fractionation on mineral modes and composition. *Lithos* 103, 309–332.
- 488 Korhonen, F.J., Saito, S., Brown, M., Siddoway, C.S., 2010. Modeling multiple melt  
489 loss events in the evolution of an active continental margin. *Lithos* 116, 230–248.
- 490 Korhonen, F. J., Brown, M., Clark, C., Bhattacharya, S., 2013. Osumilite-bearing  
491 equilibria and implications for the evolution of the Eastern Ghats Province,  
492 India. *Journal of Metamorphic Geology* 31, 881–907.
- 493 Korhonen, F.J., Brown, Clark, C., Foden, J.D., Taylor, R., 2015. Are granites and  
494 granulites consanguineous? *Geology* 43–11, 991–994.
- 495 Kunz, B.E., Johnson, T.E., White, R.W., Redler, C. 2014. Partial melting of metabasic  
496 rocks in Val Strona di Omegna, Ivrea Zone, northern Italy. *Lithos* 190–191, 1–12.
- 497 Iaccarino, S., Montomoli, C., Carosi, R., Massonne, H.-J., Visonà, D., 2017. Geology  
498 and tectono-metamorphic evolution of the Himalayan metamorphic core: insights  
499 from the Mugu Karnali transect, Western Nepal (Central Himalaya). *Journal of*  
500 *Metamorphic Geology* 35, 301–325.
- 501 Marmo, B.A., Clarke, G. L., Powell, R., 2002. Fractionation of bulk rock composition  
502 due to porphyroblast growth; effects on eclogite facies mineral equilibria, Pam  
503 Peninsula, New Caledonia. *Journal of Metamorphic Geology* 20, 151–165.
- 504 Milord, I., Sawyer, E.W., Brown, M., 2001. Formation of diatexite migmatite and  
505 granite magma during anatexis of semi-pelitic metasedimentary rocks: an example  
506 from St. Malo, France. *Journal of Petrology* 42, 487–505.
- 507 Morfin, S., Sawyer, E.W., Bandyayera, D., 2013. Large volumes of anatectic melt  
508 retained in granulite facies migmatites: an injection complex in northern Quebec.  
509 *Lithos* 168–169, 200–218.
- 510 Morrissey, L. J., Hand, M., Lane, K., Kelsey, D. E., Dutch, R. A., 2016. Upgrading  
511 iron-ore deposits by melt loss during granulite facies metamorphism. *Ore Geology*  
512 *Reviews* 74, 101–121.

- 513 Nehring, F., Foley, S., Holta, P., Van Den Kerkhof, M., 2009. Internal differentiation  
 514 of the Archean continental crust: fluid-controlled partial melting of granulites and  
 515 TTG-amphibolite associations in central Finland. *Journal of Petrology*, 50, 3–35.
- 516 Newton, R. C., Charlu, T.V., Kleppa, O.J., 1980. Thermochemistry of high structural  
 517 state plagioclases. *Geochimica et Cosmochimica Acta* 44, 933–941.
- 518 Palin, R.M., Searle, M., Waters, D.J., Horstwood, M.S.A., Parrish, R.R. 2012.  
 519 Combined thermobarometry and geochronology of peraluminous metapelites from the  
 520 Karakoram metamorphic complex, North Pakistan; New insight into the  
 521 tectonothermal evolution of the Baltoro and Hunza Valley regions. *Journal of*  
 522 *Metamorphic Geology* 30, 793–820.
- 523 Palin, R.M., Weller, O.M., Waters, D.J., Dyck, B., 2016a. Quantifying geological  
 524 uncertainty in metamorphic phase equilibrium modelling: A Monte Carlo assessment  
 525 and implications for tectonic interpretations. *Geoscience Frontiers* 7, 591–607.
- 526 Palin, R.M., White, R.W., Green, E.C.R., Diener, J.F.A., Powell, R., Holland, T. J. B.,  
 527 2016b. High-grade metamorphism and partial melting of basic and intermediate  
 528 rocks. *Journal of Metamorphic Geology* 34, 871–892.
- 529 Powell, R., Holland, J.B., 2008. On thermobarometry. *Journal of Metamorphic Geology*  
 530 26, 155–179.
- 531 Quick, J.E., Sinigoi, S., Snoke, A.W., Kalakay, T.J., Mayer, A., Peressini, G., 2003.  
 532 Geologic map of the Southern Ivrea–Verbano Zone, Northwestern Italy, Geologic  
 533 Investigations Series Map I-2776 and booklet. US Geological Survey, US  
 534 Government Printing Office, 22 pp.
- 535 Redler, C., Johnson, T.E., White, R.W., Kunz, B.E., 2012. Phase equilibrium  
 536 constraints on a deep crustal metamorphic field gradient: metapelitic rocks from the  
 537 Ivrea Zone (NW Italy). *Journal of Metamorphic Geology* 30, 235–254.
- 538 Redler, C., White, R.W., Johnson, T.E., 2013. Migmatites in the Ivrea Zone (NW  
 539 Italy): constraints on partial melting and melt loss in metasedimentary rocks from Val  
 540 Strona di Omegna. *Lithos* 175–176, 40–53.
- 541 Rolfo, F., Groppo, C., Mosca, P. 2015. Petrological constraints of the ‘Channel Flow’  
 542 model in eastern Nepal. In: Mukherjee S, Carosi R, van der Beek PA, Mukherjee BK,  
 543 Robinson DM (eds) *Tectonics of the Himalaya*. Geological Society, London, Special  
 544 Publications 412, 177–197.
- 545 Sawyer, E.W., 2008. *Atlas of Migmatites*. The Canadian Mineralogist Special  
 546 Publication 9. NRC Research Press, Ottawa, Ontario, Canada.
- 547 Sawyer, E.W., 2014. The inception and growth of leucosomes: microstructure at the  
 548 start of melt segregation in migmatites. *Journal of Metamorphic Geology* 32, 695–  
 549 712.
- 550 Sawyer, E. W., Cesare, B., Brown, M., 2011. When the continental crust melts.  
 551 *Elements*, 7, 229–234.
- 552 Schnetger, B., 1994. Partial melting during evolution of the amphibolite- to granulite  
 553 facies gneisses of the Ivrea Zone. *Chemical Geology* 113, 71–101.
- 554 Schmid, S.M., 1993. Ivrea zone and adjacent southern Alpine basement. In: V.  
 555 Raumer, J.F., Neubauer, F. (Eds.), *Pre-Mesozoic Geology in the Alps*. Springer-  
 556 Verlag, Berlin, pp. 567–583.
- 557 Stepanov, S., Hermann, J., 2013. Fractionation of Nb and Ta by biotite and phengite:  
 558 implications for the “missing Nb paradox”. *Geology* 41-3, 303–306.
- 559 Stepanov, S., Hermann, J., Rubatto, D., Korsakov, A.V., Danyushevsky, L.V., 2016.  
 560 Melting history of an ultrahigh-pressure paragneiss revealed by multiphase  
 561 solid inclusions in garnet, Kokchetav Massif, Kazakhstan. *Journal of Petrology* 57/8,  
 562 1531–1554.

- 563 Stevens, G., Villaros, A., Moyen, J.-F., 2007. Selective peritectic garnet entrainment as  
 564 the origin of geochemical diversity in S-type granites. *Geology* 35, 9–12.
- 565 Tajčmanová, L., Conolly, J.A.D., Cesare, B., 2009. A thermodynamic model for  
 566 titanium and ferric iron solution in biotite. *Journal of Metamorphic Geology* 27, 153–  
 567 165.
- 568 Taylor, J., Nicoli, G., Stevens, G., Frei, D., Moyen, J.-F., 2014. The processes that  
 569 control the leucosome composition in metasedimentary granulites: Perspectives from  
 570 the Southern Marginal Zone migmatites, Limpopo Belt, South Africa. *Journal of*  
 571 *Metamorphic Geology* 32, 713–742.
- 572 Thompson, J. B., Hovis, G. L., 1979. Entropy of mixing in sanidine. *American*  
 573 *Mineralogist* 64, 57–65.
- 574 Villaros, A., Stevens, G., Moyen, J.-F., Buick, I.S., 2009. The trace element  
 575 compositions of S-type granites: evidence for disequilibrium melting and accessory  
 576 phase entrainment in the source. *Contributions to Mineralogy and Petrology* 158,  
 577 543–561.
- 578 Wang, D., Guo, J., 2017. Late Archean high-pressure pelitic granulites in the Yinshan  
 579 Block, North China Craton. *Precambrian Research*,  
 580 <http://dx.doi.org/10.1016/j.precamres.2017.03.027>
- 581 Weinberg, R.F., Hasalová, P., 2015. Water-fluxed melting of the continental crust: a  
 582 review. *Lithos* 212–215, 158–188.
- 583 White, R.W., Powell, R., 2002. Melt loss and the preservation of granulite facies  
 584 mineral assemblages. *Journal of Metamorphic Geology* 20, 621–632.
- 585 White, R.W., Powell, R., Halpin, J.A., 2004. Spatially-focussed melt formation in  
 586 aluminous metapelites from Broken Hill, Australia. *Journal of Metamorphic Geology*  
 587 22, 825–845.
- 588 White, R.W., Powell, R., Holland, T.J.B., 2007. Progress relating to calculation of  
 589 partial melting equilibria for metapelites. *Journal of Metamorphic Geology* 25, 511–  
 590 527.
- 591 White, R.W., Palin, R.M., Green, E.C.R., 2017. High-grade metamorphism and partial  
 592 melting in Archean composite grey gneiss complexes. *Journal of Metamorphic*  
 593 *Geology* 35, 181–195.
- 594 Yakymchuk, C., Brown, M., 2014. Consequences of open-system melting in tectonics.  
 595 *Journal of the Geological Society* 171, 21–40.
- 596 Yakymchuk, C., Brown, M., Clark, C., Korhonen, F.J., Piccoli, P.M.,  
 597 Siddoway, C. S., . . . Vervoort, J. D. 2015. Decoding polyphasemigmatites using  
 598 geochronology and phase equilibria modeling. *Journal of Metamorphic Geology* 33,  
 599 203–230.
- 600 Zeng, L., Saleeby, J.B., Asimow, P., 2005. Nd isotope disequilibrium during crustal  
 601 anatexis: A record from the Goat Ranch migmatite complex, southern Sierra Nevada  
 602 batholith, California. *Geology* 33, 53–56.

#### 603 CAPTIONS:

604  
 605  
 606 Fig. 1: Schematic  $P$ – $T$  diagram showing the formation of nanogranitoid inclusions in  
 607 anatexitic rocks. After onset of melting, the growing peritectic mineral traps droplets of  
 608 melt produced by melting reaction. Along cooling path, melt inclusions partially to  
 609 totally crystallize into a cryptocrystalline aggregate (nanogranitoid).

610  
 611 Fig. 2: Melt-reintegration approach for the residual migmatite IZ070 (Ivrea Zone).  
 612 White dots indicate  $P$ – $T$  conditions where melt was reintegrated. The chosen chemical

613 system is NCKFMASHT. Red line: solidus. Yellow line: muscovite-out curve. Light  
 614 blue field: region where liquid H<sub>2</sub>O is predicted. Labels referring to the bulk rock  
 615 compositions used in the modeling are reported in parenthesis (see Table 1). *P–T* path  
 616 reconstructed from Redler et al. (2013).

617  
 618 Fig. 3: Harker plots (wt.%) showing the final model protolith compositions (anhydrous  
 619 compositions from Table 1) obtained (i) by reintegrating melt inclusion compositions  
 620 and (ii) by Redler et al. (2013) applying the original melt-reintegration method  
 621 proposed by White et al. (2004). Bulk rock compositions of granulite- and  
 622 amphibolite-facies metapelites are from Redler et al. (2013).

623  
 624 Fig. 4: Calculated mineral and melt abundance along prograde paths of Figs. 1a and  
 625 S3.

626  
 627 Fig. 5: Contours for  $X_{Mg}$  (Mg/(Mg+Fe)) value of biotite, for  $X_{An}$  (Ca/(Ca+Na)) of  
 628 plagioclase and for almandine component of garnet, for pseudosections in Figures 1a  
 629 and S3. Continuous and dotted lines as in Fig. 4.

630  
 631 Fig. 6: Bivariant diagrams (wt.%) comparing anhydrous compositions of reintegrated  
 632 nanogranitoid inclusions (squares; Table 1) and melts calculated at the same conditions  
 633 (ellipses). Grey arrows indicate increasing *P–T* conditions. Black lines connect  
 634 calculated composition (white star) with the corresponding melt inclusion composition  
 635 (black star) from Ronda diatexites (data from Bartoli et al., 2016b). See text for details.

636  
 637 Fig. 7: Sketch of two different modes of occurrence of nanogranitoid inclusions in  
 638 anatectic rocks. (a) Garnet from Himalaya in which hundreds of melt inclusions (black  
 639 dots) show a systematic distribution in an annulus around a nanogranitoid-free core  
 640 (see Carosi et al., 2015; Cesare et al., 2015; Rolfo et al., 2015). (b) Garnet from Ronda  
 641 area (Betic Cordillera, Spain) containing two different types of nanogranitoid  
 642 inclusions. Inclusions corresponding to a H<sub>2</sub>O-poor leucogranitic melt (black dots)  
 643 coexist with rutile and kyanite at the garnet core, whereas H<sub>2</sub>O-rich granodioritic to  
 644 tonalitic melt inclusions (blue dots) are present towards garnet rim along with  
 645 sillimanite and ilmenite (see Barich et al., 2014; Acosta-Vigil et al., 2016).

646  
 647 Table 1: Bulk rock and melt compositions (wt.%) used in the phase equilibria  
 648 modeling.

## 649 650 651 **Appendix A. Supplementary data**

652  
 653 Fig. S1: Schematic map of Val Strona di Omegna (redrawn from Redler et al., 2012,  
 654 2013). The locality of the residual granulite IZ070 used for the calculations is given.

655  
 656 Fig. S2: Bivariant diagrams (wt%) comparing bulk rock compositions of migmatites  
 657 and granulites containing melt inclusions used in this study (data from Bartoli, 2017;  
 658 Bartoli et al., 2016a; Barich et al., 2014) and granulite IZ070 from Val Strona di  
 659 Omegna.

660  
 661  
 662 Fig. S3: Phase equilibria modeling considering the bulk composition IZ070Re obtained

663 by Redler et al. (2013). The chosen chemical system is NCKFMASHT. Red line:  
664 solidus. Yellow line: muscovite-out curve. Light blue field: region where liquid H<sub>2</sub>O is  
665 predicted.

ACCEPTED MANUSCRIPT

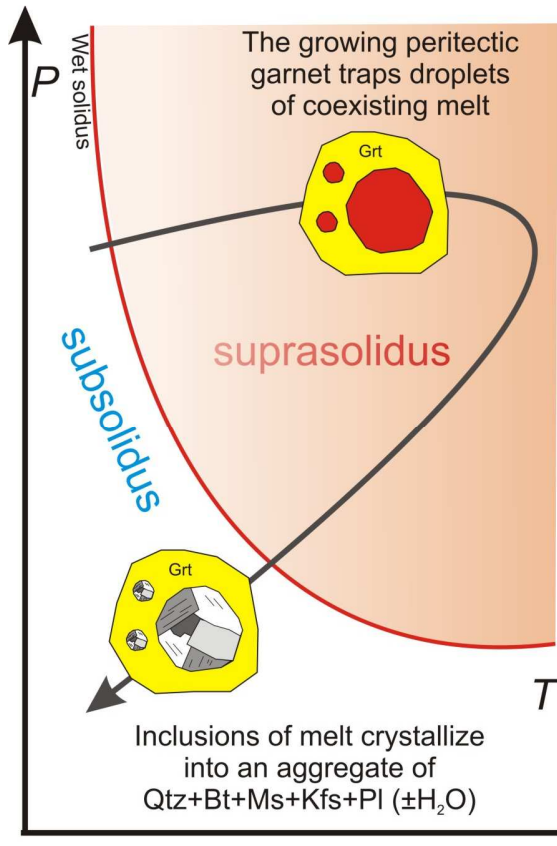


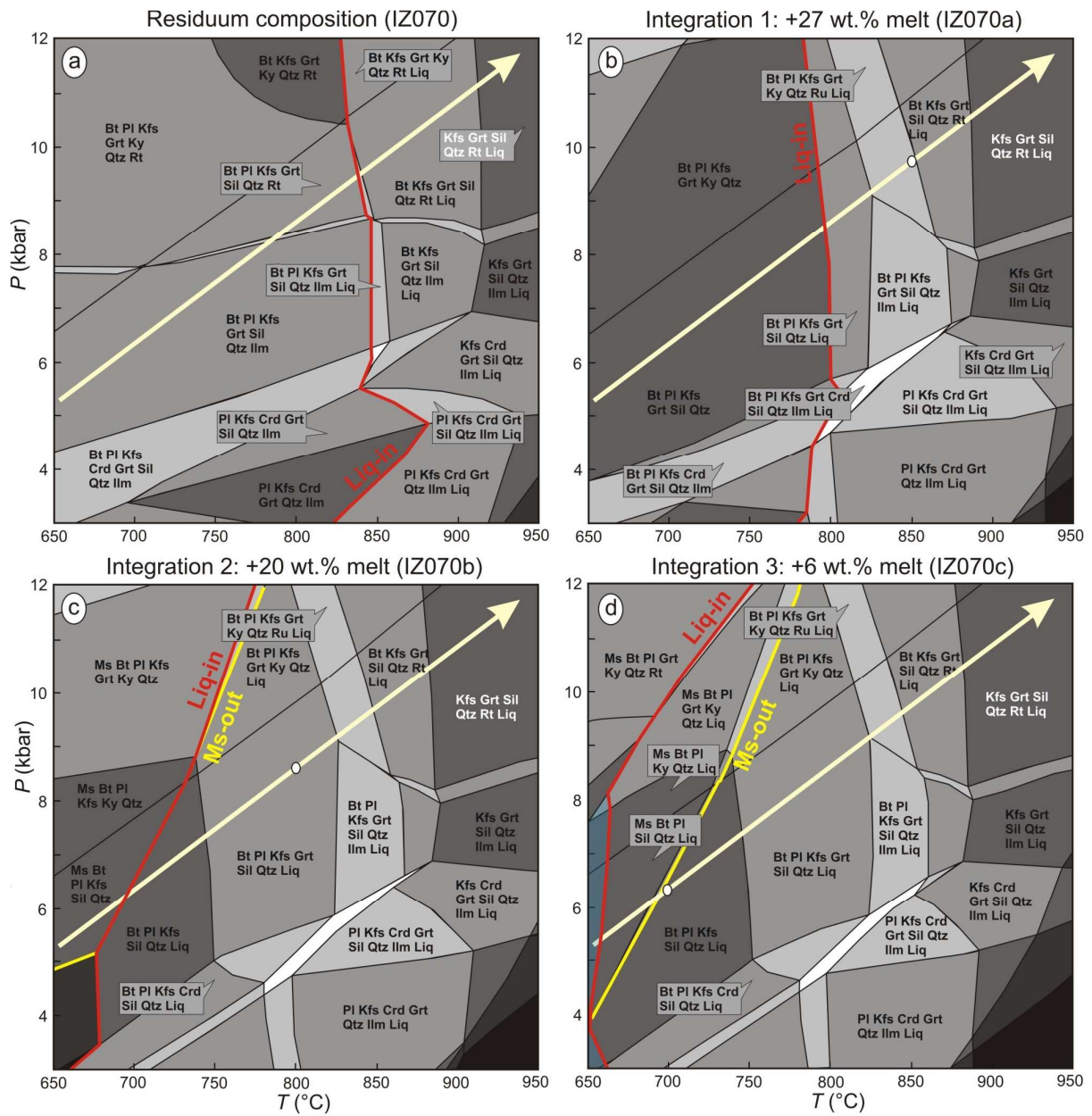
**Table 1.** Bulk rock and compositions (wt.%) used in the modeling.

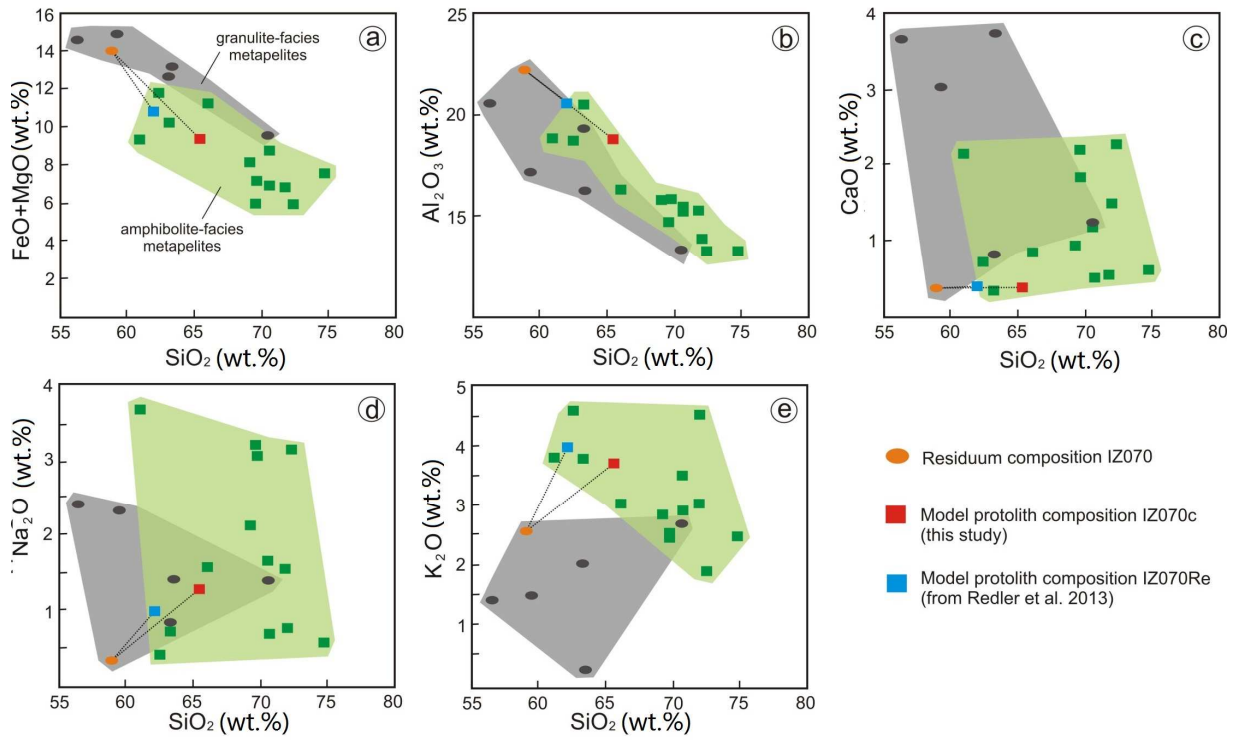
Label	Bulk rock composition					Melt inclusion composition**		
	IZ070*	IZ070a	IZ070b	IZ070c	IZ070Re*	≈700 °C	≈800 °C	≈850 °C
Temp.								
No. analyses						240	53	79
SiO <sub>2</sub>	58.74	61.90	64.09	64.62	61.20	72.80	74.55	73.58
TiO <sub>2</sub>	1.39	1.11	0.92	0.88	1.04	0.08	0.05	0.08
Al <sub>2</sub> O <sub>3</sub>	22.13	20.35	18.93	18.56	20.27	12.51	13.30	13.78
FeO	10.58	8.67	7.49	7.12	8.10	1.21	1.47	1.59
MgO	3.49	2.78	2.31	2.23	2.64	0.14	0.14	0.15
CaO	0.30	0.41	0.36	0.34	0.38	0.26	0.35	0.82
Na <sub>2</sub> O	0.34	0.88	1.18	1.26	0.97	2.83	2.79	2.90
K <sub>2</sub> O	2.58	3.16	3.62	3.65	3.94	4.88	5.12	5.29
H <sub>2</sub> O	0.45	0.74	1.09	1.34	1.45	5.29	2.23	1.81
Tot.	100.00	100.00	100.00	100.00	99.99	100.00	100.00	100.00

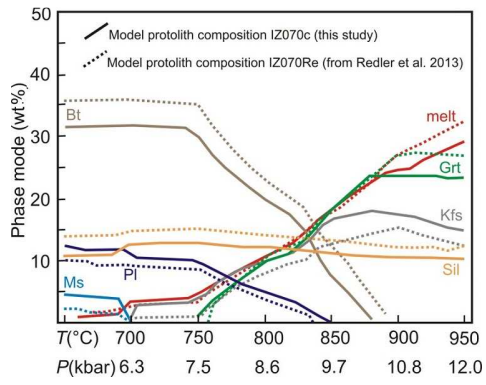
\* From Redler et al. (2013)

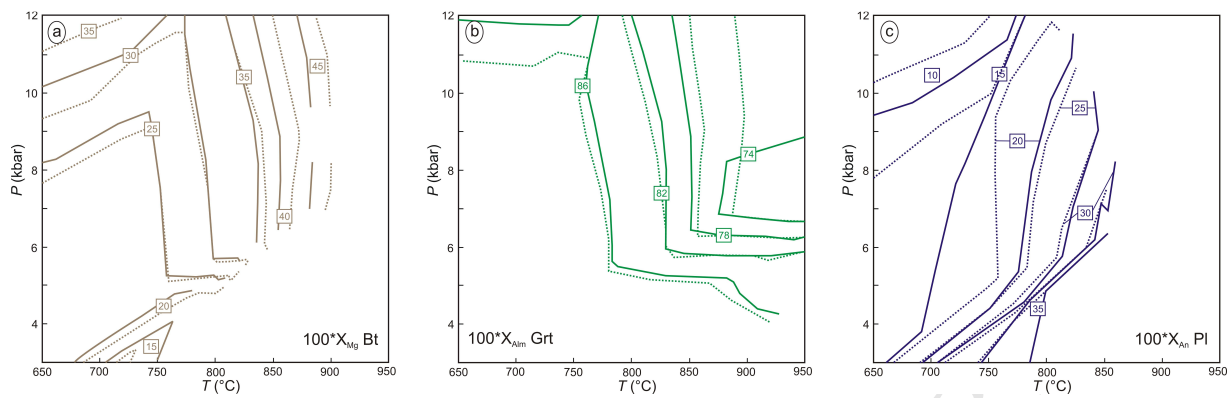
\*\* From Cesare et al. (2015), Bartoli et al. (2016)

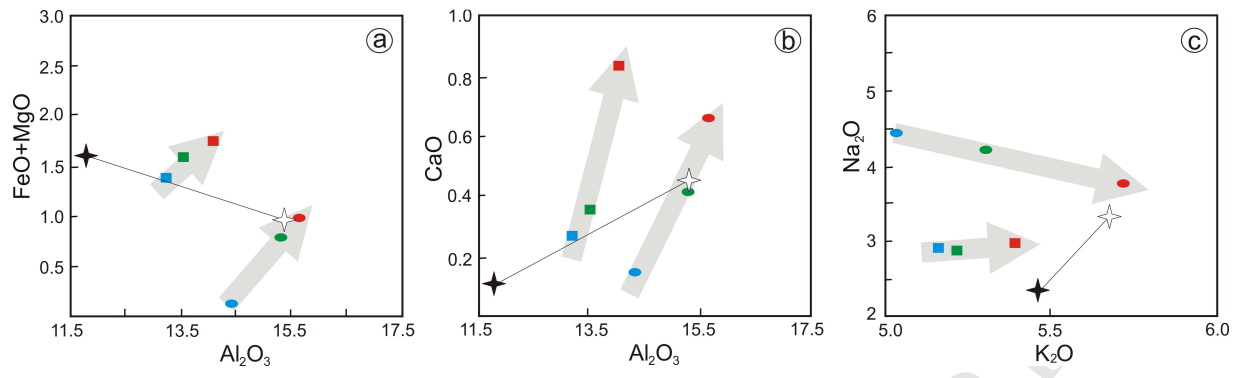


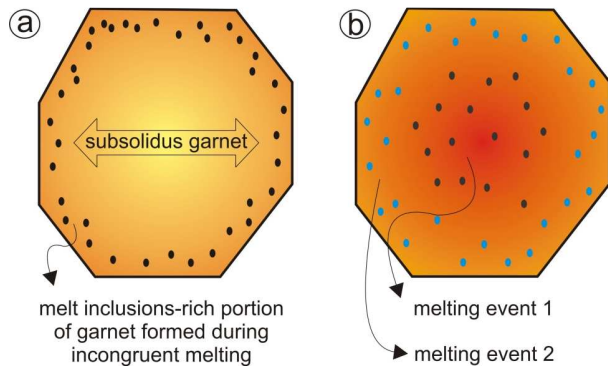












ACCEPTED MANUSCRIPT



- Nanogranitoid inclusions have the potential to provide the primary composition of crustal melts at the source
- A novel use of the nanogranitoid compositional database is presented here
- Reintegrating melt inclusion compositions from the published database into residual rock compositions can be a further useful method to reconstruct a plausible prograde history of melt-depleted rocks